Splitting of Van Hove singularities in slightly twisted bilayer graphene

Si-Yu Li, Ke-Qin Liu, Long-Jing Yin, Wen-Xiao Wang, Wei Yan, Xu-Qin Yang, Jun-Kai Yang, Haiwen Liu, Hua Jiang, and Lin He

Phys. Rev. B **96**, 155416 — Published 6 October 2017

DOI: 10.1103/PhysRevB.96.155416

Splitting of Van Hove singularities in a slightly twisted bilayer graphene

Si-Yu Li[1,2], Ke-Qin Liu[1,2], Long-Jing Yin[1,2], Wen-Xiao Wang[1,2], Wei Yan[1,2], Xu-Qin Yang[1,2], Jun-Kai Yang[1,2], Haiwen Liu[1,2], Hua Jiang[3,*], and Lin He[1,2,*]

[1]Center for Advanced Quantum Studies, Beijing Normal University, Beijing, 100875, People's Republic of China

[2]Department of Physics, Beijing Normal University, Beijing, 100875, People's Republic of China

[3]College of Physics, Optoelectronics and Energy, Soochow University, Suzhou, 215006, People's Republic of China

Correspondence and requests for materials should be addressed to H.J. (e-mail: jianghuaphy@suda.edu.cn) and L.H. (e-mail: helin@bnu.edu.cn).

A variety of new and interesting electronic properties have been predicted in graphene monolayer doped to Van Hove singularities (VHSs) of its density-of-state. However, tuning the Fermi energy to reach a VHS of graphene by either gating or chemical doping is prohibitively difficult, owning to their large energy distance (~ 3 eV). This difficulty can be easily overcome in twisted bilayer graphene (TBG). By introducing a small twist angle between two adjacent graphene sheets, we are able to generate two low-energy VHSs arbitrarily approaching the Fermi energy. Here, we report experimental studies of electronic properties around the VHSs of a slightly TBG through scanning tunneling microscopy measurements. The split of the VHSs is observed and the spatial symmetry breaking of electronic states around the VHSs are directly visualized. These exotic results provide motivation for further theoretical and experimental studies of graphene systems around the VHSs.

I. INTRODUCTION

In the past few years, twisted bilayer graphene (TBG), a system with a twist angle between two adjacent graphene sheets, has been intensively studied [1-18]. It exhibits many novel electronic properties that distinct from the electronic properties of graphene monolayer and Bernal bilayer. For example, the TBG has angle dependent low-energy Van Hove singularities (VHSs) [1,3-6] and Fermi velocity renormalization [15,16], and it can exhibit energy dependent chiral tunneling [9] and exotic quantum Hall effect [2,17,18]. Among all these unique electronic properties, the low-energy VHSs, which originate from the two low-energy saddle points in the band structures, have attracted much attention over the years in the studies of the TBG. Previously, it was predicted that graphene could exhibit novel correlated states when the Fermi level is close to the VHSs of graphene monolayer [19-25]. Unfortunately, the VHSs of graphene monolayer are too far (~ 3 eV) to be reached in experiment [26]. Therefore, an experimental study of electronic properties at the VHSs of graphene is still lacking up to now. The TBG systems with small twist angles open up new prospects in this direction because their low-energy VHSs are fully accessible with the present doping and gating techniques.

Here we show that by reducing the twist angle, it is possible to tune the VHSs of the TBG arbitrarily approaching the Fermi energy. When the VHSs is tuned close to the Fermi level, we observe the split of the VHSs and the distortion of electronic states around the VHSs. Such a result indicates that the TBG can exhibit novel electronic properties around the VHSs.

II. EXPERIMENT

The TBG was grown on a 25 micron thin Rh foil via a traditional ambient pressure chemical vapor deposition (CVD) method [4] and the growth processes are shown in Supplementary Fig. 1 [27]. The Rh foil was firstly heated from room temperature to 1000 ºC in 30 min under an Ar flow of 850 sccm and a hydrogen gas flow of 100 sccm. Then the furnace was held at the same gas environment for 60 min at 1000 ºC. Finally, CH_4 gas was introduced with a flow ratio of 5 sccm, and the growth time is varied from 3 to 15 min for controlling the thickness of graphene. The sample was then slowly cooled down to room temperature.

The scanning tunneling microscopy (STM) system was an ultrahigh vacuum single-probe scanning probe microscope (USM-1300) from UNISOKU with magnetic fields up to 15 T. All STM and scanning tunneling spectroscopy (STS) measurements were performed at liquid-helium temperature (~4.2 K) and the images were taken in a constant-current scanning mode. The STM tips were obtained by chemical etching from a wire of Pt(80%) Ir(20%) alloys. Lateral dimensions observed in the STM images were calibrated using a standard graphene lattice as well as a Si (111)-(7×7) lattice. The STS spectra were calibrated using an Ag (111) surface. The STS spectrum (the *dI/dV-V* curve) was carried out with a standard lock-in technique by applying alternating current modulation of the bias voltage (871 Hz) to the tunneling bias. The energy resolution of our experiment is limited by both the temperature ($\sim 3k_BT \approx 1$ meV, where k_B is the Boltzmann constant and T~4.2 K) and the oscillation of bias voltage added in quadrature. The STS spectra of low spectroscopic resolution were carried out

with lock-in oscillation 7 mV applying to the tunneling bias, which limits the energy resolution to around 10 meV. In order to acquire the spectra with high spectroscopic resolution, we lower the oscillation of lock-in bias voltage to 0.7 mV by using 1/10 bias divider during the STS measurement, where the energy resolution of high-resolution spectra is improved to about 1 meV.

The STS images are used to reflect the spatial distribution of local density-of-state (LDOS) at fixed sample bias. The STS image is acquired by measuring the dI/dV at fixed sample bias on each pixel of the area. In this case, the feedback loop is closed when the tip stops on the fixed position to take bias spectroscopy measurement. During the process that the tip moves to the next position, the feedback loop is changed to open in order to keep the distance between the tip and the sample almost fixed.

II. Results and analysis

Splitting of the VHSs in a slightly TBG. In our experiment, graphene bilayers were synthesized by CVD on Rh foils and we have demonstrated previously that the graphene bilayers on Rh foils have a strong twisting tendency [4,12,28]. Therefore, such a system provides an ideal platform for twist engineering of the low-energy VHSs. Figure 1(a) shows a schematic structure of two misoriented graphene sheets with a twist angle θ. The period D of the twist-induced moiré pattern is related to θ by $D = a/[2\sin(\theta/2)]$ with $a = 0.246$ nm the lattice constant of graphene. Figure 1(b) shows a representative STM image of a twisted bilayer with the period $D \approx 11.3$ nm. The twist angle is estimated to be $\theta \approx 1.2^{o}$.

As schematically shown in Fig. 1(a), the twisting not only results in the moiré

pattern, but also leads to a relative shift of the two Dirac cones $|\Delta \boldsymbol{K}| = 2|\boldsymbol{K}|\sin(\theta/2)$, where $\boldsymbol{K}$ is the reciprocal-lattice vector, in reciprocal space. A finite interlayer coupling between the two graphene sheets leads to the emergence of two saddle points appearing at the intersections of the two Dirac cones, which consequently generate two low-energy VHSs in the DOS, as shown in Fig. 1(c) for the theoretical LDOS of the TBG with twist angle $\theta \approx 1.2^{o}$ (see Supplementary Fig. 2 for calculation details [27]). The upper panel of Fig. 1(d) shows a typical STS spectrum of the TBG with the energy resolution of about 10 meV (see Supplementary Fig. 3(a) for more spectra with the similar energy resolution). The energy difference of $\Delta E_{VHS} \approx 25$ meV of the two VHSs peaks, as shown in the upper panel of Fig. 1(d), agrees well with both our theoretical result in Fig. 1 (c) and that reported in previous experimental work with a similar twist angle [3-6]. However, by carefully measuring the spectra with a high spectroscopic resolution of around 1 meV (see Experiment section for more details about the high-resolution STS measurements), as shown in the lower panel of Fig. 1(d), we observe a completely new feature of the VHSs: each of the VHSs splits into two peaks with energy separation of about 10 meV. The splitting of the VHSs, which has never been reported before in the TBG, only depends slightly on the positions of the moiré pattern (see Supplementary Fig. 3(b) [27]).

STM characterizations of the TBG. To further explore the origin of the splitting of the VHSs, we measure the structure of the TBG at varying voltage bias. Figure 2(a) and 2(b) show two typical STM images recorded at voltage bias away from and around the VHSs, respectively (see Supplementary Fig. 4 for more STM images

recorded at different sample bias [27]). Obviously, the obtained structures of the moiré patterns in these STM images are quite different. For the STM image recorded at bias (i.e., at energy) around the VHSs (Fig. 2(b)), there is an obvious structural deformation of the moiré patterns along a preferential direction over large scale. However, the twist-induced moiré patterns exhibit much weaker structural deformation when we measure the STM image at voltage bias (i.e., at energy) away from the VHSs, as shown in Fig. 2(a). We can rule out the tip effect as the origin of the deformation of the moiré pattern [29] because the shape of the moiré patterns does not show dependence on the varying currents in our STM measurements (see Supplementary Fig. 5 for STM images measured on various currents [27]). To quantitatively describe the deformation, we use the full width at half maximum (FWHM) of the scanning profile lines across the moiré patterns in x and y directions, i.e., L_x and L_y, to represent the shape of the moiré patterns (see Supplementary Fig. 6(a) [27]). Figure 2(c) and 2(d) show the measurements of the L_x and L_y on the moiré patterns at the energies of 100 meV and -8.5 meV, respectively (see Supplementary Fig. 6(b) and (c) for the measurements at other energies). Figure 2(f) summarizes the ratio of L_y/L_x averaged for tens of the moiré patterns as a function of the voltage bias. Obviously, the symmetry of the moiré patterns is seriously broken when the energy of the TBG is close to the low-energy VHSs. In the STM images, both topography and electronic states of the sample contribute to the contrast. To explore the origin of the deformation of the moiré patterns, we carry out atomic resolution STM measurements of the moiré patterns, as shown in Fig. 2(e) (also see Supplementary Fig. 7 for details

[27]). These measurements demonstrate that the lattice distortion in the moiré patterns is negligible, indicating that the observed distortion in the moiré patterns is mainly contributed by the electronic effects at the energies around the VHSs. The distortion of the electronic states, which are strongly related to the electron-electron interactions magnified by the enhanced DOS around the VHSs [18-24,30], could be directly measured by STS maps and will be discussed subsequently.

Symmetry breaking of electronic states around the VHSs. Differential conductance maps (STS maps), which are widely used to directly reflect the spatial distribution of the LDOS [3,6,31-35], are further measured to study the electronic states of the TBG in our experiment. The presence of the moiré pattern in the TBG is expected to lead to spatial variation of the LDOS. Figure 3(a) and 3(b) show representative STS maps recorded at energies away from the VHSs of the TBG with $\theta \approx 1.2^{o}$. The distribution of the LDOS (Fig. 3(a) and 3(b)) reveals the same period and circular symmetry of the moiré pattern but exhibits the inverted contrast comparing with that shown in the STM image (Fig. 1(b)). Such a result is reproduced well in our theoretical simulations, as shown in Fig. 3(c) and 3(d), reflecting the presence of the moiré potential in the twist-induced moiré pattern [13,14,34]. Similar LDOS distribution over the moiré pattern is also observed in the TBG with slightly large twist angles, for example in the TBG with $\theta \approx 1.9^{o}$ (D = 7.3 nm) in our experiment, as shown in Fig. 4(a) and 4(b) (see Supplementary Fig. 11 for STM image and STS spectrum of the sample [27]). Around the VHSs of the 1.9^{o} sample, the distribution of the LDOS also shows the same period and circular symmetry of the moiré pattern, as

shown in Fig. 4(c) and 4(d). However, the spatial-distribution of the LDOS around the VHSs exhibits the same contrast as the moiré pattern in the STM image, which is the slight difference comparing with that measured away from the VHSs. The said result is also reproduced quite well by our theoretical calculations (without taking into account the electron-electron interactions), as shown in Fig. 5(a) and 5(b).

In the TBG with $\theta \approx 1.2^{o}$, the spatial distribution of the LDOS at VHSs is expected to be affected due to the splitting of the VHSs (i.e., the enhanced electron-electron interactions around the low-energy VHSs). Such an effect can be directly visualized through the STS maps in our STM measurements. Figure 5(c)-5(f) show STS maps recorded at the four peaks of the VHSs in the TBG with $\theta \approx 1.2^{o}$, exhibiting pronounced spatial modulation of the LDOS. Quite different from the LDOS distribution recorded at energies away from the VHSs (Fig.3), both the period and the symmetry of the moiré pattern are completely removed from the spatial distribution of the LDOS at the VHSs. The distortion of electronic states observed in Fig. 5(c)-(f) cannot be induced by the tip effect on STS maps [33] because that similar effect has not been observed in other TBG measured in the same experimental conditions (see Supplementary Fig. 11 for further discussion [27]).

IV. Discussion

Recently, similar splitting of DOS peaks has been observed around monovacancy and isolated hydrogen atoms on graphene and is attributed to the enhanced electron-electron interactions because the intensity of the localized DOS increases dramatically when the monovacancy or the isolated hydrogen atom is approached

[36,37]. Therefore, the observed splitting of the VHSs indicates the lifting of degenerate electronic states at the VHSs, which may be induced by an enhanced electron-electron interaction when the VHSs approach the Fermi level. Very recently, electronic transport measurements really show evidences of electron-electron interactions in a slightly TBG [38]. Here we should point out that the small twist angle is vital in the enhanced electron-electron interactions around the VHSs in the TBG because of the following two main aspects. First, the VHSs are approaching the charge neutrality point of the system and also the Fermi level in our experiment with decreasing twist angles (see Fig. 1(d) and the inset of Fig. 2(f)). Second, the magnitude of the DOS at the VHSs increases and the FWHM of the VHSs decreases with decreasing twist angles (the inset of Fig. 2(f)). Therefore, the electron-electron interactions are expected to be more significant for the TBG with small twist angles. To verify such a result, controlled experiments on several TBG with different twist angles are carried out. In the TBG with larger twist angles (the VHSs are more than 100 meV away from the Fermi energy), we do not observe obvious deformation of the moiré patterns at the energy of VHSs and the corresponding splitting of the VHSs in the same STM measurements (see Fig. 2(f) and Supplementary Figs. 8-11 for the results of other TBG samples with different twist angles [27]). The above controlled experiments also help us to remove possible effects of the STM tip and the supporting substrate as the origin of the observed phenomena.

In our experiment, the observed spatial distribution of LDOS around the VHSs no longer follows the periodicity of the moiré pattern. The observed distorted electronic

states around the VHSs of the TBG are quite different from the charge-density-wave (CDW) reported previously [39-41]. For the CDW, the LDOS would have a periodicity associated with some features of the sample [39-41]. The distortion of the periodicity and the symmetry of the LDOS around the VHSs has never been reported before and seems beyond current understanding of electronic properties of the TBG. Although further studies are needed to fully understand the distortion of the periodicity and the symmetry of the LDOS, our experiment demonstrates that it affects the contrast in the STM images, resulting in the deformation of the moiré patterns recorded around the VHSs. More importantly, the spatial symmetry breaking of the LDOS lifts the degenerate electronic states at the VHSs and results in the observed splitting of the VHSs.

In the TBG with small twist angles, there is pronounced Fermi velocity renormalization [15,16] and the Fermi velocity will reduce to about zero when $\theta \approx 1.1^{o}$. Therefore, the quasiparticles are strongly localized in the TBG with $\theta \approx 1.2^{o}$. This is also very important for the emergence of the correlated states because the ratio of the interaction energy compared to the kinetic energy is expected to increase dramatically around the VHSs of this TBG. By applying a magnetic field up to 13 T, we still cannot observe Landau quantization (Fig. 6) since the picture of two-dimensional free electron gas no longer applies in the TBG with $\theta \approx 1.2^{o}$. Such a result consists with the previous observations for the slightly TBG in STM measurements [6,15,16]. However, quantum Hall effects are still observed in the slightly TBG through transport measurements [17,18,38]. At present, the exact reason

for this discrepancy is still not known and needs to be further explored. The different methods in the experiment may be the possible origin: In the STM measurements, the spectra are recorded in the interior of the TBG; whereas, in the transport measurements, the quantum Hall effects are contributed by the edges of the slightly TBG, where the translation symmetry of the sample is broken. The strong magnetic fields affect slightly the tunneling spectra (Fig. 6) and the spatial distribution of the LDOS in the TBG, as shown in Fig. 7. Such a result is reasonable and easy to be understood since that there may be a competition between twist-induced localization and cyclotron motion generated by the large perpendicular magnetic fields. The magnetic length $l_B = \sqrt{\hbar / eB}$ generated by the magnetic field of 13 T is estimated to be about 7 nm, which is much smaller than the period of the moiré patterns, ~ 11.3 nm, in the TBG with $\theta \approx 1.2^o$.

IV. CONCLUSIONS

In summary, the observation of the splitting of the VHSs and the distorted spatial distribution of the LDOS around the VHSs indicate the important effects of electron-electron interactions at the VHSs in the graphene moiré superlattice. Our result provides a new route to realize novel correlated states in graphene systems in the near future.

Appendix:

Theoretical studies for the twist bilayer Graphene.

In this section, we detail the numerical studies for energy spectrum, LDOS and

spatial distribution of LDOS in the twisted bilayer Graphene, following the techniques developed previously [1,7]. Supplementary Fig. 13 plots the unit cell for a typical twisted bilayer Graphene. The two unit vectors are $\vec{L}_1 = m\vec{a}_1 + n\vec{a}_2$ and $\vec{L}_2 = -n\vec{a}_1 + (m+n)\vec{a}_2$ with $\vec{a}_1 = a(1,0)$ and $\vec{a}_2 = a(\frac{1}{2}, \frac{\sqrt{3}}{2})$. Here, a = 0.246 nm is the lattice constant. The twist is modeled by the clockwise commensurable rotation from $\vec{L}_1$ to vector $\vec{L}_1' = n\vec{a}_1 + m\vec{a}_2$. After some simple algebras, one obtain the period of Moir□é pattern $|L| = a\sqrt{m^2 + n^2 + mn}$, the number of atoms in a unit cell $N = 4(m^2 + mn + n^2)$, and the twist angle

$$\theta = 2\sin^{-1}\frac{m-n}{2\sqrt{m^2+n^2+mn}} \quad . \tag{1}$$

According to above equation, the twist angle θ = 1.2º, 1.7º, 2.1º, 2.6º, 3.1º correspond to (m, n) = (27, 26), (20, 19), (16, 15), (13, 12), (11, 10).

In the tight-binding representation, the Hamiltonian for the twisted bilayer graphene is written as:

$$\begin{aligned} \mathrm{H} &= \mathrm{H_T} + \mathrm{H_B} + \mathrm{H}_{int} \\ \mathrm{H}_{T/B} &= -\sum_{<i,j>} \mathrm{t} c_i^+ c_j + h.c. \\ \mathrm{H}_{int} &= -\sum_{i\in T}\sum_{j\in B} t_{ij} c_i^+ c_j + h.c. \end{aligned} \quad , \tag{2}$$

where $\mathrm{H_T}$, $\mathrm{H_B}$, $\mathrm{H_{int}}$ represent Hamiltonian for the top layer, the bottom layer and the coupling between these two layers, respectively. c_i^+ denotes the creation operator for electron on site r_i. The nearest neighbor intra-layer hopping energy is t = 2.7 eV. The inter-layer hopping energy between site r_i and r_j is given by

$$t_{ij} = t_{\perp} e^{-\frac{|r_i - r_j| - d_0}{\xi}}, \quad (3)$$

where the parameters are set as $t_{\perp} = -0.46\ \mathrm{eV}$, $d_0 = 0.335$ nm, $\xi = 0.0453$ nm. Under such parameters, the energy level spacing between the two main van Hove singularity is about 24 meV at $\theta = 1.2^{\circ}$, in consistent with the experiment.

Next, by performing the Fourier transformation to H, one can obtain the momentum space Hamiltonian H(k). Then, the energy eigenvalue E_k and corresponding eigenstate $\phi_k(r_i)$ is found by diagonalizing H(k). Thus, the energy spectrum of twisted bilayer graphene can be obtained. Moreover, the LDOS and spatial distribution of LDOS are calculated from

$$\rho(E) = \sum_k \delta(E - \varepsilon_k)$$

$$\rho(E, r_i) = \sum_k \delta(E - \varepsilon_k) \left|\phi_k(r_i)\right|^2 \quad . \quad (4)$$

Both $\rho(E)$ and $\rho(E, r_i)$ are numerical obtained by Monte Carlo method with no less than 10000 random k in the first Brillouin zone are counted. In order to compare the LDOS behaviors at difference θ, we have set $\rho(E = 1\ \mathrm{eV})$ as the reference unit.

References

1. Lopes dos Santos, J. M. B., Peres, N. M. R., Castro Neto, A. H. Graphene bilayer with a twist: electronic structure. *Phys. Rev. Lett.* **99**, 256802 (2007).
2. Shallcross, S., Sharma, S., Pankratov, O. A. Quantum Interference at the Twist Boundary in Graphene. *Phys. Rev. Lett.* **101**, 056803 (2008).
3. Li, G., Luican, A., Lopes dos Santos, J. M. B., Castro Neto, A. H., Reina, A., Kong, J., Andrei, E. Y. Observation of Van Hove singularities in twisted

graphene layers. *Nature Phys*. **6**, 109-113 (2009).

4. Yan, W., Liu, M., Dou, R.-F., Meng, L., Feng, L., Chu, Z.-D., Zhang, Y., Liu, Z., Nie, J.-C., He, L. Angle-dependent van Hove singularities in a slightly twisted graphene bilayer. *Phys. Rev. Lett*. **109**, 126801 (2012).
5. Brihuega, I., Mallet, P., Gonzalez-Herrero, H., Trambly de Laissardiere, G., Ugeda, M. M., Magaud, L., Gomez-Rodriguez, J. M., Yndurain, F., Veuillen, J.-Y. Unraveling the Intrinsic and Robust Nature of van Hove Singularities in Twisted Bilayer Graphene by Scanning Tunneling Microscopy and Theoretical Analysis. *Phys. Rev. Lett*. **109**, 196802 (2012).
6. Yin, L.-J., Qiao, J.-B., Zuo, W.-J., Li, W.-T., He, L. Experimental evidence for non-Abelian gauge potentials in twisted graphene bilayers. *Phys. Rev. B* **92**, 081406(R) (2015).
7. Suarez Morell, E., Correa, J. D., Vargas, P., Pacheco, M., Barticevic, Z. Flat bands in slightly twisted bilayer graphene: tight-binding calculations. *Phys. Rev. B* **82**, 121407(R) (2010).
8. Ohta, T., Robinson, J. T., Feibelamn, P. J., Bostwick, A., Rotenberg, E., Beechem, T. E. Evidence for Interlayer Coupling and Moiré Periodic Potentials in Twisted Bilayer Graphene. *Phys. Rev. Lett*. **109**, 186807 (2012).
9. He, W.-Y., Chu, Z.-D. & He, L. Chiral Tunneling in a Twisted Graphene Bilayer. *Phys. Rev. Lett.* **111**, 066803 (2013).
10. Bistritzer, R. & MacDonald, A. H. Moire bands in twisted double-layer graphene. *Proc Natl Acad Sci* (*USA*) **108**, 12233-12237 (2011).

11. San-Jose, P., Gonzalez, J., Guinea, F. Non-Abelian gauge potentials in graphene bilayers. *Phys. Rev. Lett.* **108**, 216802 (2012).

12. Yan, W., Meng, L., Liu, M., Qiao, J.-B., Chu, Z.-D., Dou, R.-F., Liu, Z., Nie, J.-C., Naugle, D. G., He, L. Angle-dependent van Hove singularities and their breakdown in twisted graphene bilayers. *Phys. Rev. B* **90**, 115402 (2014).

13. Chu, Z.-D., He, W.-Y., He, L. Coexistence of van Hove singularities and superlattice Dirac points in a slightly twisted graphene bilayer. *Phys. Rev. B* **87**, 155419 (2013)

14. Wong, D., Wang, Y., Jung, J., Pezzini, S., DaSilva, A. M., Tsai, H., Jung, H. S., Khajeh, R., Kim, Y., Lee, J., Kahn, S., Tollabimazraehno, S., Rasool, H., Watanabe, K., Taniguchi, T., Zettl, A., Adam, S., MacDonald, A. H., Crommie, M. F. Local spectroscopy of moiré-induced electronic structure in gate-tunable twisted bilayer graphene. *Phys. Rev. B* **92**, 155409 (2015).

15. Luican, A., Li, G., Reina, A., Kong, J., Nair, R. R., Novoselov, K. S., Geim, A. K., Andrei, E. Y. Single-Layer Behavior and Its Breakdown in Twisted Graphene Layers. *Phys. Rev. Lett.* **106**, 126802 (2011).

16. Yin, L.-J., Qiao, J.-B., Wang, W.-X., Zuo, W.-J., Yan, W., Xu, R., Dou, R.-F., Nie, J.-C., He, L. Landau quantization and Fermi velocity renormalization in twisted graphene bilayers. *Phys. Rev. B* **92**, 201408(R) (2015).

17. Kim, Y., Herlinger, P. Moon, P., Koshino, M., Taniguchi, T., Watanabe, K., Smet, J. H. Charge inversion and topological phase transition at a twist angle induced van Hove singularity of bilayer graphene. *Nano Lett.* **16**, 5053 (2016).

18. Rode, J. C., Smirnov, D., Schmidt, H., Haug, R. J. Berry phase transition in twisted bilayer graphene. *2D Mater.* **3**, 035005 (2016).

19. González, J. Kohn-Luttinger superconductivity in graphene. *Phys. Rev. B* **78**, 205431 (2008).

20. Martin, I., Batista, C. D. Itinerant electron-driven chiral magnetic ordering and spontaneous quantum Hall effect in triangular lattice models. *Phys. Rev. Lett.* **101**, 156402 (2008).

21. Nandkishore, R., Levitov, L. S., Chubukov, A. V. Chiral superconductivity from repulsive interactions in doped graphene. *Nature Phys*. **6**, 158-263 (2010).

22. Wang W. S., Xiang Y. Y., Wang Q. H., Wang F., Yang F., and Lee D. H., Functional renormalization group and variational Monte Carlo studies of the electronic instabilities in graphene near 1/4 doping. *Phys. Rev. B* **85**, 035414 (2012).

23. González, J. Magnetic and Kohn-Luttinger instabilities near a Van Hove singularity: Monolayer versus twisted bilayer graphene. *Phys. Rev. B* **88**, 125434 (2013).

24. McChesney, J. L., Bostwick, A., Ohta, T., Seyller, T., Horn, K., González, J., Rotenberg, E. Extended van Hove Singularity and Superconducting Instability in Doped Graphene. *Phys. Rev. Lett.* **104**, 136803 (2010).

25. Roberts, A. T., Binder, R., Kwong, N. K., Golla, D., Cormode, D., LeRoy, B. J., Everitt, H. O., Sandhu, A. Optical characterization of electron-phonon interactions at the saddle point in graphene. *Phys. Rev. Lett.* **112**, 187401 (2014).

26. Castro Neto, A. H., Guinea, F., Peres, N. M. R., Novoselov, K. S., Geim, A. K. The electronic properties of graphene. *Rev. Mod. Phys.* **81**, 109 (2009).

27. See Supplemental Material for methods, more STM images, STS spectra, and details of the calculations.

28. Yan, W., He, W.-Y., Chu, Z.-D., Liu, M., Meng, L., Dou, R.-F., Zhang, Y., Liu, Z., Nie, J.-C., He, L. Strain and curvature induced evolution of electronic band structures in twisted graphene bilayer. *Nature Commun.* **4**, 2159 (2013).

29. Yankowitz, M., Watanabe, K., Taniguchi, T., San-Jose, P., LeRoy, B. J. Pressure-induced commensurate stacking of graphene on boron nitride. *Nature Commun.* **7**, 13168 (2016).

30. Cao, Y., Luo, J. Y., Fatemi, V., Fang, S., Sanchez-Yamagishi, J. D., Watanabe, K., Taniguchi, T., Kaxiras, E., Jarillo-Herrero, P. Superlattice-induced insulating states and valley-protected orbits in twisted bilayer graphene. *Phys. Rev. Lett.* **117**, 116804 (2016).

31. Yazdani, A, da Silva Neto, E. H., Aynajian, P. Spectroscopic imaging of strongly correlated electronic states. *Annual Review of Condensed Matter Physics* 7, 11 (2016)

32. Yankowitz, M., Wang, J. J., Li, S., Birdwell, A. G., Chen, Y.-A., Watanabe, K., Taniguchi, T., Quek, S. Y., Jarillo-Herrero, P., LeRoy, B. J. Band structure mapping of bilayer graphene via quansiparticle scattering. *APL material* **2**, 092503 (2014).

33. da Silva Neto, E. H., Aynajian, P., Baumbach, R. E., Bauer, E. D., Mydosh, J.,

Ono, S., Yazdani, A. Detection of electronic nematicity using scanning tunneling microscopy. *Phys. Rev. B* **87**, 161117(R) (2013).

34. Yankowitz, M., Xue, J., Cormode, D., Sanchez-Yamagishi, J. D., Watanabe, K., Taniguchi, T., Jarillo-Herrero, P., Jacquod, P., LeRoy, B. J. Emergence of superlattice Dirac points in graphene on hexagonal boron nitride. *Nature Phys*. **8**, 382-386 (2012).
35. Yin, L.-J., Jiang, H., Qiao, J.-B. & He, L. Direct imaging of topological edge states at a bilayer graphene domain wall. *Nature Commun.* **7**, 11760 (2016).
36. Gonzalez-Herrero, H. *et al.* Atomic-scale control of graphene magnetism by using hydrogen atoms. *Science* **352**, 437-441 (2016).
37. Zhang, Y. *et al.* Scanning tunneling microscopy of the π magnetism of a single carbon vacancy in graphene. *Phys. Rev. Lett.* **117**, 166801 (2016).
38. Kim, K., DaSilva, A., Huang, S., Fallahazad, B., Larentis, S., Taniguchi, T., Watanabe, K., Leroy, B. J., MacDonald, A. H., Tutuc, E. Tunable Moiré Bands and Strong Correlations in Small-Twist-Angle Bilayer Graphene. *Proc Natl Acad Sci* (*USA*) **114**, 3364-3369 (2017).
39. Carpinelli, J. M., Weitering, H. H., Plummer, E. W., Stumpf, R. Direct observation of a surface charge density wave. *Nature* **381**, 398-400 (1996).
40. Wise, W. D., Boyer, M. C., Chatterjee, K., Kondo, T., Takeuchi, T., Ikuta, H., Wang, Y., Hudson, E. W. Charge-density-wave origin of cuprate checkerboard visualized by scanning tunnelling microscopy. *Nature Phys*. **4**, 696-699 (2008).
41. Barja, S., Wickenburg, S., Liu, Z.-F., Zhang, Y., Ryu, H., Ugeda, M. M, Hussain,

Z., Shen, Z.-X., Mo, S.-K., Wong, E., Salmeron, M. B., Wang, F., Crommie, M. F., Ogletree, D. F., Neaton, J. B., Weber-Bargioni, A. Charge density wave order in 1D mirror twin boundaries of single-layer $MoSe_2$. *Nature Phys*. **12**, 751-756 (2016).

Acknowledgments

This work was supported by the National Natural Science Foundation of China (Grant Nos. 11674029, 11422430, 11374035, 11374219, 11504008), the National Basic Research Program of China (Grants Nos. 2014CB920903, 2013CBA01603, 2014CB920901), the NSF of Jiangsu province, China (Grant No. BK20160007), the program for New Century Excellent Talents in University of the Ministry of Education of China (Grant No. NCET-13-0054). L.H. also acknowledges support from the National Program for Support of Top-notch Young Professionals and support from "the Fundamental Research Funds for the Central Universities".

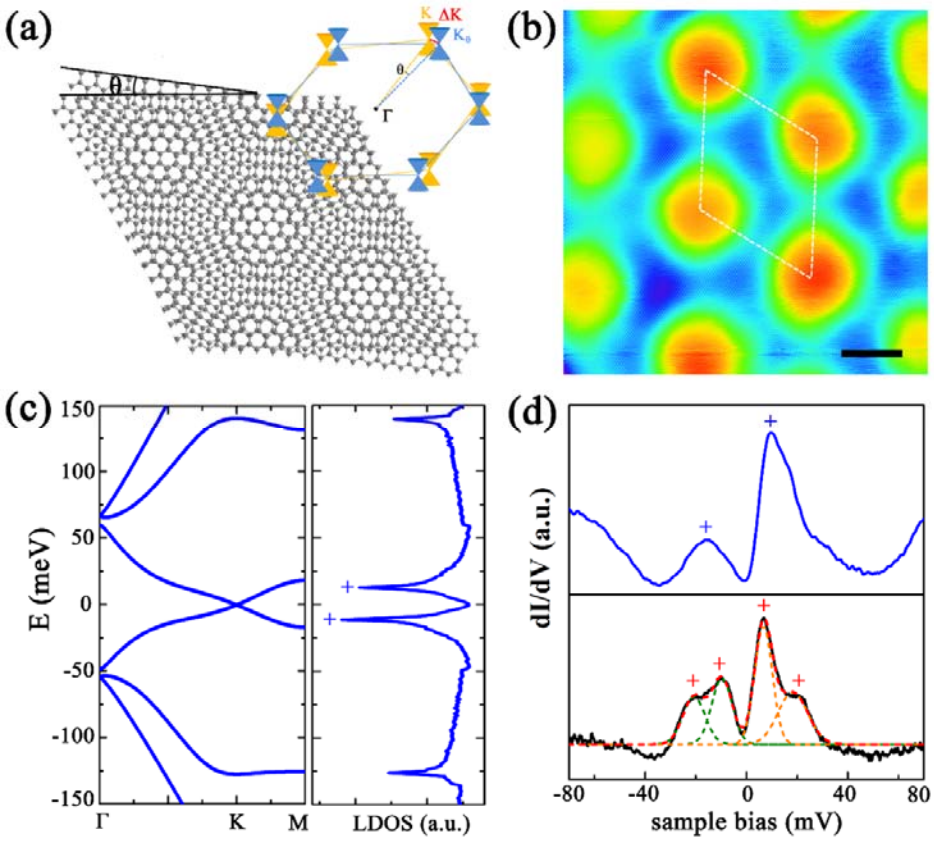

Figure 1. The splitting of VHSs in the TBG with twist angle $\theta \sim 1.2°$. **(a).** Schematic structure of two misoriented graphene sheets with a twist angle θ and schematic two Dirac cones, K and K_θ, of the two layers intersect in momentum space. **(b).** A 30 nm × 30 nm STM image of the TBG with the period D ~ 11.3 nm and the twist angle $\theta \sim 1.2°$ (V_{sample} = -78 mV and I = 0.4 nA). Scale bar: 5 nm. **(c)**. Theoretical calculated electronic structure of the TBG with twist angle $\theta \sim 1.2°$ and the corresponding LDOS with VHS peaks. **(d)**. Upper panel: low-resolution STS spectrum of the TBG in (b), with the energy resolution of about 10 meV. Lower panel: a typical high-resolution STS spectrum of the same TBG with energy resolution of around 1

meV. Each of the two VHSs splits into two peaks and the dashed lines mark the result of Gaussian fitting for the split VHSs.

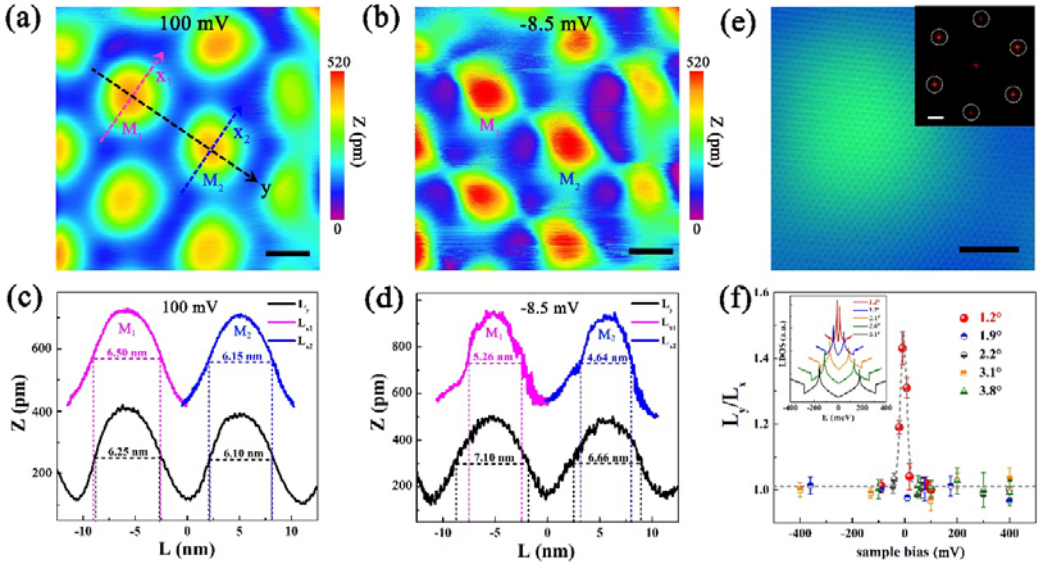

Figure 2. Deformation of the moiré superlattice around VHSs. **(a), (b).** The 30 nm × 30 nm STM images recorded at voltage bias 100 mV and -8.5 mV respectively (I = 0.2 nA). Scale bar: 5 nm. **(c), (d).** The scanning profile lines across the moiré patterns M_1 and M_2 in x and y direction at the energies of 100 meV (c) and -8.5 meV (d), respectively. The measured directions y, x_1 and x_2 are marked in (a). And the numbers correspond to the measured FWHM values of the profile lines. For clarity, we stack the profile lines by y offsets. **(e).** The atomic-resolution STM image of the moire pattern (V_{sample} = 300 mV and I = 0.3 nA). Scale bar: 1 nm. Inset show the corresponding 2D Fourier transform image. The six bright spots marked by the white dashed circles correspond to the reciprocal lattices of graphene. Scale bar: 10 nm^{-1}. **(f).** Summarization for the ratio of L_y/L_x as a function of the voltage bias for several TBG samples with different twist angles, where L_x and L_y are the FWHM of the moiré patterns along x and y directions respectively. The gray dashed line is the Gaussian

fitting between the L_y/L_x of TBG with twist angle $\theta\sim1.2°$ and the voltage bias. Inset: theoretical calculated LDOS as the function of energy E in the TBG with different twist angles.

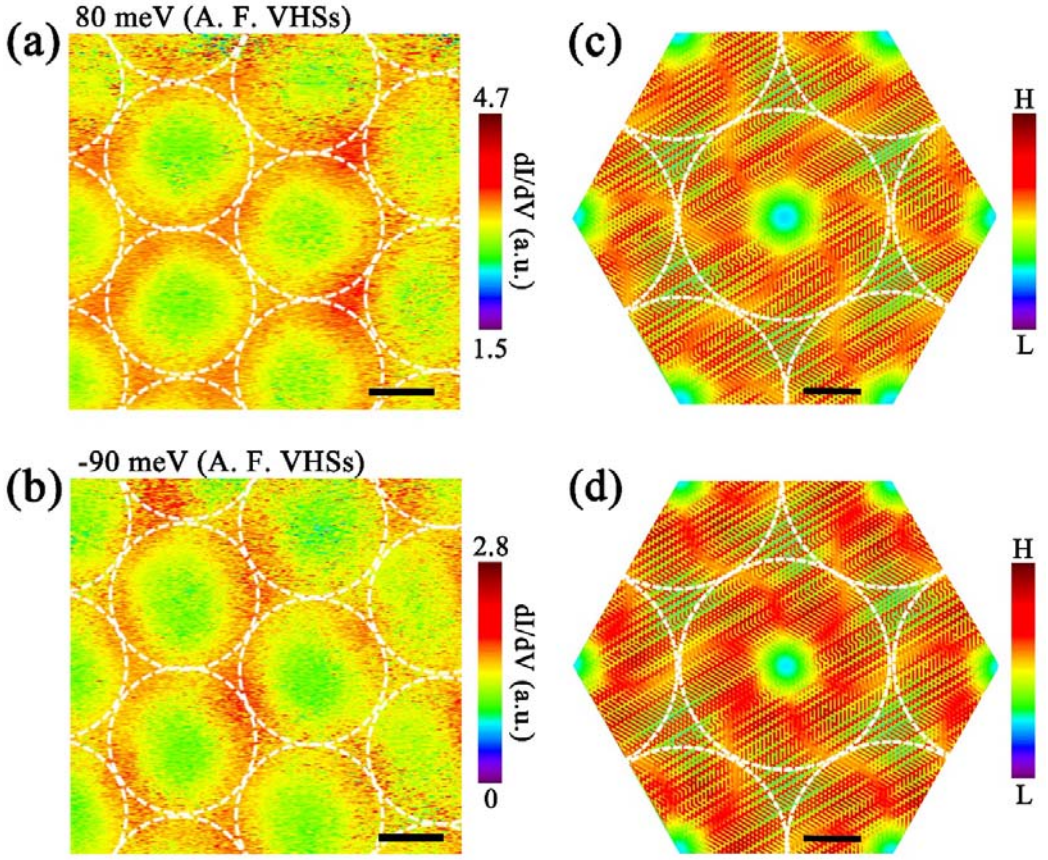

Figure 3. Spatial distribution of the LDOS away from the VHSs (A. F. VHSs for short) in the TBG. **(a), (b).** Experimental STS maps recorded in the TBG with twist angle $\theta\sim1.2°$ at the fixed sample bias of 80 mV in (a) and -90 mV in (b), respectively. Scale bar: 5 nm. The white dashed circles mark the period and circular symmetry of the moiré patterns in STM image. **(c), (d).** Theoretically spatial distribution of the LDOS at the energies away from the VHSs, i.e., 139 meV in (c) and -126 meV in (d), in the TBG with twist angle $\theta\sim1.2°$. Scale bar: 3 nm.

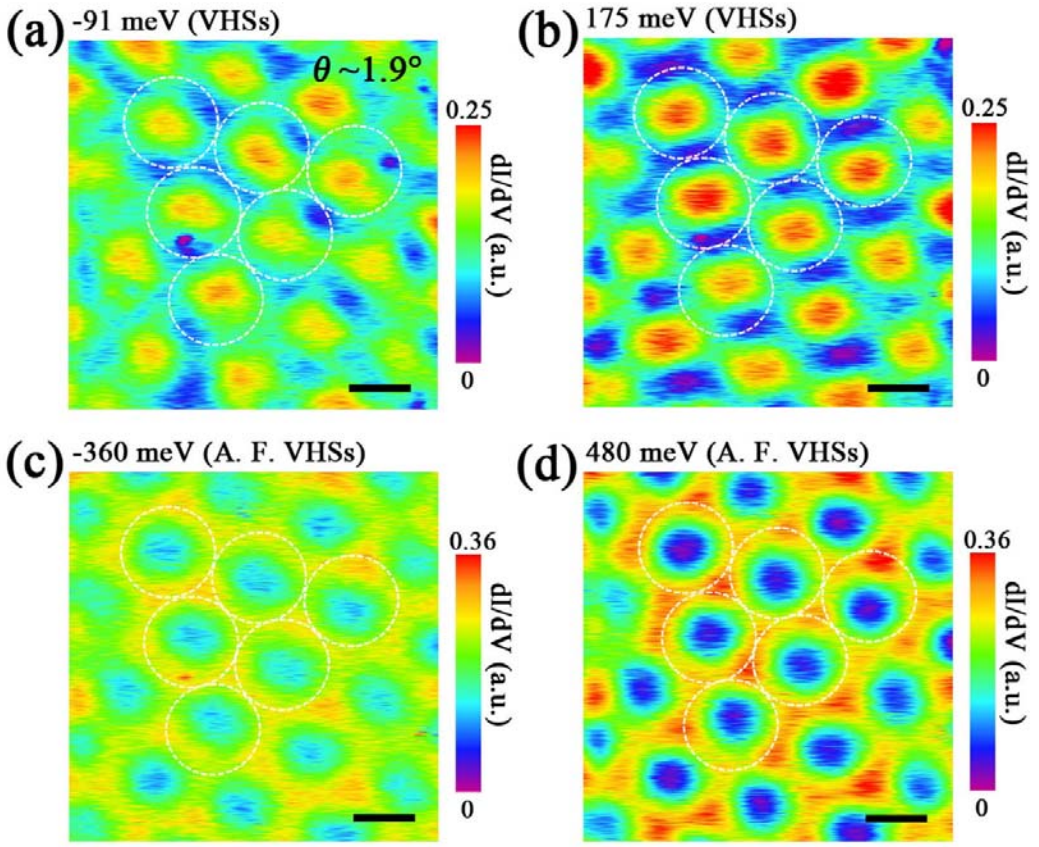

Figure 4. Conductance maps of the TBG with the period of D~7.3 nm and twist angle θ~1.9°. **(a), (b).** STS maps of the TBG with the fixed sample bias around the VHS peaks, i.e., -91 mV and 175 mV, which shows the spatial distribution of LDOS following the same period and circular symmetry with the moiré superlattice in STM image. Scale bar: 5 nm. The white dashed circles mark the period and circular symmetry of the moiré patterns in STM image. **(c), (d).** STS maps of the TBG recorded at the energies of the second dips -360 meV and 480 meV respectively. Their spatial LDOS distributions show the same circular period with moire pattern but the inverted contrast comparing with the STM image. Scale bar: 5 nm.

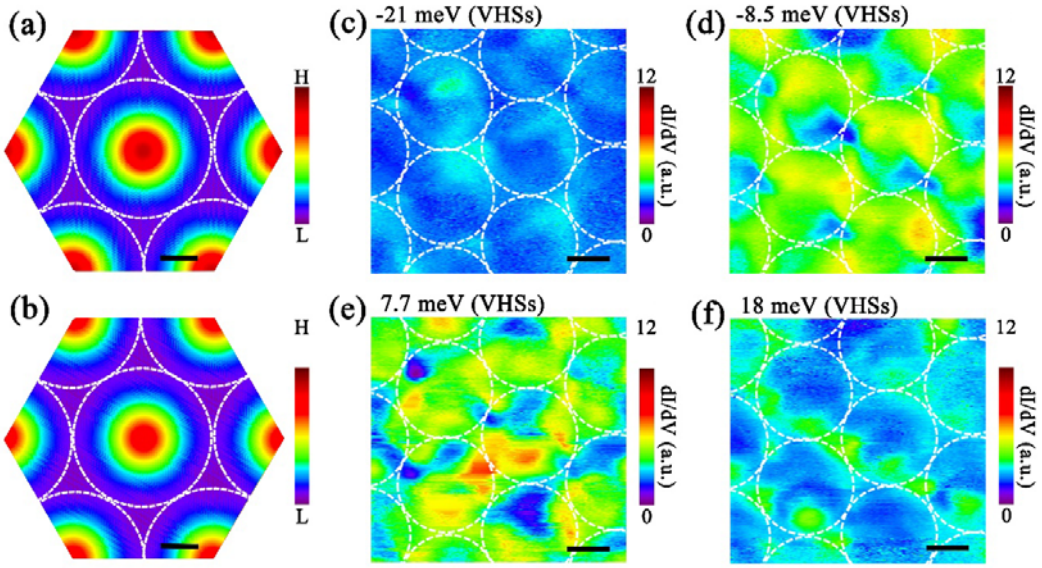

Figure 5. Distortion of the electronic states around the VHSs of the TBG with twist angle $\theta \sim 1.2°$. **(a), (b).** Theoretical spatial distribution of the LDOS in the TBG with twist angle $\theta \sim 1.2°$ at the energies of the two VHSs in the calculated LDOS (Fig. 1(c)), respectively. Scale bar: 3 nm. **(c)-(f).** Experimental STS maps recorded in the same region of the TBG at the fixed sample bias -21 mV, -8.5 mV, 7.7 mV and 18 mV, respectively, which correspond to the four split VHSs in lower panel of Fig. 1(d). Scale bar: 5 nm. The white dashed circles mark the period and circular symmetry of the moiré superlattice in the STM image.

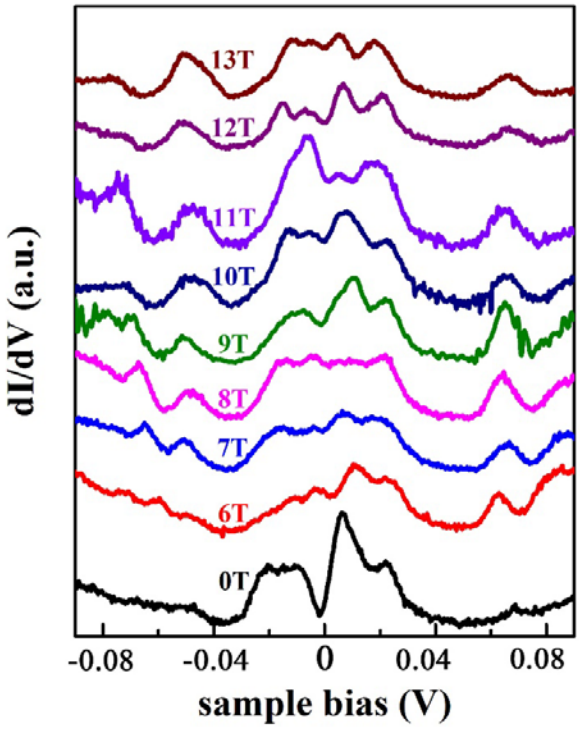

Figure 6. High-resolution STS spectra taken from the TBG with twist angle $\theta \sim 1.2°$ under different magnetic fields. All the spectra show the splitting VHSs.

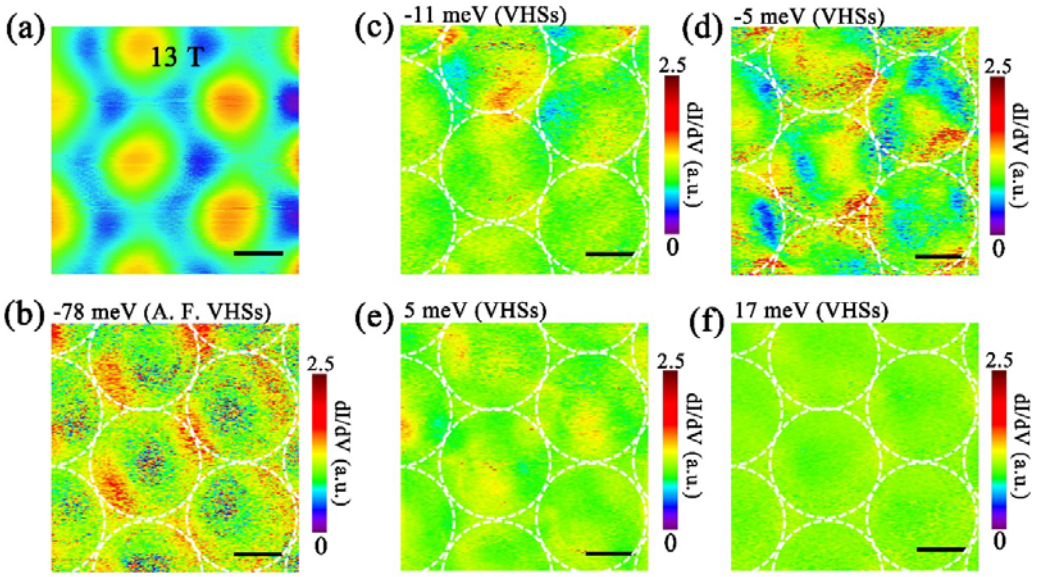

Figure 7. (a). A 30 nm × 30 nm STM image of the TBG with twist angle $\theta \sim 1.2°$ (V_{sample} = 120 mV and I = 0.2 nA) under 13T. Scale bar: 5 nm. **(b).** STS map of the

TBG with the fixed sample bias of -78 mV under 13T. **(c)-(f).** STS maps recorded in the same region of the TBG with the fixed sample bias, i.e., -11 mV, -5 mV, 5 mV and 17 mV under 13T respectively, corresponding to the four split VHSs. Scale bar: 5 nm. The white dashed circles mark the period and circular symmetry of the moiré patterns.